HHS Public Access

Author manuscript

Curr Opin Chem Biol. Author manuscript; available in PMC 2019 August 01.

Published in final edited form as:

Curr Opin Chem Biol. 2018 August ; 45: 95–103. doi:10.1016/j.cbpa.2018.03.015.

Emergence of Two Near-Infrared Windows for In-Vivo and Intraoperative SERS

Lucas A. Lane[1,*], **Ruiyang Xue**[2], and **Shuming Nie**[1,2,*]

[1]Department of Biomedical Engineering, College of Engineering and Applied Sciences, Nanjing University, Nanjing, China

[2]Departments of Bioengineering, Chemistry, Electrical and Computer Engineering, and Materials Science and Engineering, University of Illinois at Urbana-Champaign, Urbana, Illinois, USA

Abstract

Two clear windows in the near-infrared (NIR) spectrum are of considerable current interest for in-vivo molecular imaging and spectroscopic detection. The main rationale is that near-infrared light can penetrate biological tissues such as skin and blood more efficiently than visible light because these tissues scatter and absorb less light at longer wavelengths. The first clear window, defined as light wavelengths between 650 nm and 950 nm, has been shown to be far superior for in-vivo and intraoperative optical imaging than visible light. The second clear window, operating in the wavelength range of 1000 nm to 1700 nm, has been reported to further improve detection sensitivity, spatial resolution, and tissue penetration because tissue photon scattering and background interference are further reduced at longer wavelengths. Here we discuss recent advances in developing biocompatible plasmonic nanoparticles for in-vivo and intraoperative surface-enhanced Raman scattering (SERS) in both the first and second NIR windows. In particular, a new class of “broad-band” plasmonic nanostructures is well suited for surface Raman enhancement across a broad range of wavelengths allowing a direct comparison of detection sensitivity and tissue penetration between the two NIR window. Also, optimized and encoded SERS nanoparticles are generally nontoxic and are much brighter than near-infrared quantum dots (QDs), raising new possibilities for ultrasensitive detection of microscopic tumors and image-guided precision surgery.

Graphical abstract

[*]Authors to whom correspondence should be addressed: lucaslane@nju.edu.cn; nies@illinois.edu.

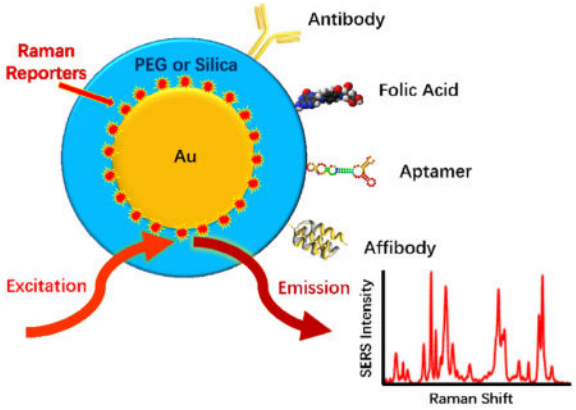

2. Introduction

Surface enhanced Raman scattering (SERS) continues to garner great interest for use in biology and medicine owing to having signals of exceptional sensitivity and specificity [1,2]. In particular, SERS offers many favorable properties that are well suited for in-vivo molecular imaging and spectroscopic detection. In contrast to fluorescence, SERS signals are much more stable against photobleaching [3,4], and their peak widths are often less than a few nanometers [5]. The spectral signatures from Raman scattering are unique, allowing an unmistakable discrimination between target and background signals [6,7]. SERS nanoparticle probes, otherwise known as SERS nanotags, have simple constructions consisting of a metallic core, a Raman reporter giving a unique spectral signature, and a coating for biocompatibility and linkage to bioaffinity molecules or targeting ligands (see Figure 1A). Changing the spectral signature can be simply performed by changing the Raman reporter [8,9], thereby avoiding complicated chemistries that are often required for spectral changes in fluorescence probes. SERS probes with different spectral signatures can all be excited at a single wavelength and detected with simple instrumentation for multiplexing. In contrast to organic NIR fluorophores that are often limited by poor quantum yields and low extinctions [10], strong SERS spectra can be obtained at near-infrared wavelengths with ultrahigh sensitivity and specificity (reaching detection limits of femtomolar to attomolar levels) [6]. Such detection limits far exceed that of current imaging modalities such as fluorescence, optical coherence tomography (OCT), magnetic resonance imaging (MRI), x-ray computed tomography (CT), and positron emission tomography (PET). In addition, SERS nanotags are considerably brighter and much more photostable in comparison with organic dyes and fluorescent proteins (Figure 1B).

As depicted in Figure 1C–E, two clear windows for in-vivo optical imaging exist in the NIR window (650 – 1700 nm) of the optical spectrum [10,11]. Wavelengths in the visible spectrum (< 650 nm) have very limited penetration into tissues, as visible light is heavily absorbed and scattered [12,13], and suffers from extensive background autofluorescence from tissue chromophores [14]. Moreover, increased scattering of light limits both spatial resolution and signal-to-background ratios due to more photons migrating away from the main path between excitation and emission sources. On the other end of the window,

wavelengths greater than 1700 nm are affected by increased losses due to water absorption [10]. The NIR window is further broken down into two regions, classified as the first (650–900 nm) and second (1000–1700 nm) NIR windows. The demarcation within 900 – 1000 nm is mainly due to the spectral bounds of CCD detectors made of either silicon (Si) or indium gallium arsenide (InGaAs), where the detection quantum efficiency drops after 900 nm for silicon and arises abruptly after 1000 nm for indium gallium arsenide (Figure 1C).

3. SERS in the First NIR Window

In-vivo SERS studies started with instrumentation in the first NIR window due to readily available and cost-effective dispersive Raman systems using 785 nm diode lasers and silicon CCD detectors having high speed and detection sensitivity. Nie and coworkers were the first to use biocompatible SERS nanotags for in-vivo tumor detection applications [15]. They developed SERS tags having superior brightness over organic fluorophores and quantum dots, and demonstrated their use for in-vivo tumor identification. Additionally, they observed that adding targeting ligands to the nanoparticle surface did not increase the total accumulation of nanoparticles to tumor, but rather kept nanoparticles localized within the tumor for a longer period of time. This finding challenged the previously held belief that adding targeting ligands could increase nanoparticle uptake within solid tumors [16]. Soon after, Gambhir and coworkers demonstrated the great multiplexing power of in-vivo SERS imaging, showing ten different signatures of SERS tags could be simultaneously identified [8]. Since these pioneering reports, there has been an increasing number of publications using SERS techniques for in-vivo applications, primarily focusing on cancer imaging and detection. Nanoparticles have preferential accumulation within tumors due to the tumor physiological characteristics of leaky vasculature and impaired lymphatics, otherwise known as the enhanced permeability and retention (EPR) effect [17,18]. However, unlike other imaging techniques using nanoparticles, SERS can detect microscopic tumors at the single-cell sensitivity level, providing a unique advantage in aiding surgical resections of residual tumors and metastatic lymph nodes. Survival for many cancer patients depends strongly on a complete resection which requires a surgeon to see the entire scope of tumor infiltration within surrounding normal tissues, including microscopic metastatic legions. In a typical SERS guided surgical procedure, SERS tags are injected intravenously and are allowed to circulate and hone to cancer cells for a period of several hours, after which the tumor area is inspected with a handheld fiberoptic device that excites and collects the signal from the SERS tags (Figure 2) [19,20]. Resecting under the guidance of SERS signals, the surgeon can remove the primary tumors and satellite metastatic legions completely, sparing normal or healthy tissues.

A recent noteworthy advance in precision tumor detection using SERS tags has been reported by Kircher and colleagues [7]. They demonstrated the use of SERS tags having 1.5 fM sensitivity to detect tumors in models of pancreatic, breast, and prostate cancers along with sarcomas. This study showed that bright SERS tags could be used to not only determine primary tumor margins, but also microscopic tumor foci invading into surrounding tissues and micrometastatic legions. Interestingly, these SERS tags were also able to identify precancerous legions. The targeting of SERS particles to both microscopic cancerous and precancerous legions was believed to arise from accelerated macropinocytotic uptake at

these regions. Small or microscopic tumor legions are less likely to have lymphatic impairment, so their retention cannot be explained by the EPR effect. Similar observations of enhanced internalization by cancer cells have also been reported for nano-sized ICG-albumin complexes [21], a common fluorophore used in fluorescence guided surgery. A major feature of this enhanced cellular uptake mechanism is that it is applicable to many cancer types, thus avoiding the need for targeting agents, which tend to be limited as they only target particular cancer cell subtypes. In general, the concentrations of internalized SERS particles are low within malignant and premalignant cells, but spectroscopic detection is still possible due to the brightness of SERS nanotags. The same group has also developed Raman reporters with exceptionally strong signals, offering detection limits at the attomolar level [6], potentially allowing the detection of a single cancer cell. The ability to precisely determine tumor margins and identify small legions from many cancer types is a compelling reason for developing SERS nanoparticles for future clinical use.

4. SERS in the Second NIR Window

Though the first NIR window offers better tissue penetration than visible wavelengths, more favorable optical conditions can be met by moving towards longer wavelengths inside the second NIR window. Major benefits of operating in the second NIR window arise mainly from further reductions in absorbance, scattering, and the autofluorescence background [22–27]. Less absorbance leads to less heating, for instance the maximal permissible intensity applied to the skin at 1064 nm is 3.4 times higher than 785 nm [28]. Tissue light scattering is considerably reduced at longer wavelengths as it scales with $^{-a}$, where a ranges between 0.2 – 4 [10,13]. Fluorescence by tissue chromophores also decreases exponentially at longer wavelengths reaching undetectable levels beyond 1500 nm [29–31].

Investigations of in-vivo SERS in the second NIR window are just beginning to be reported. Traditional FT-Raman systems operating in the second NIR window were inadequate for in-vivo studies due to limitations in sensitivity, speed, and spatial resolution. However, newer dispersive technologies using low-loss spectrographs and high-sensitivity InGaAs CCDs are starting to become more cost-effective and readily available. As a result, researchers are currently developing SERS tags that are active within this region. We note that at these longer wavelengths, it becomes increasingly important to have both the particle’s plasmonic absorption and Raman reporter in resonance with the excitation wavelength, leading to exceptional SERS enhancements [32]. Plasmon resonances are tuned with the degree of anisotropy of the particle [33–37]. Anisotropic particles that support plasmons throughout the NIR region include nanorods [38–40], nanobipyramids [41–43], nanocages [44–46], nanoshells [47–50], nanotriangles [51–53], nanostars [54–58], and nanomatryoshkas [59,60].

A significant amount of work in advancing SERS tags into the second NIR window has been performed by Graham and colleagues. They have designed hollow gold nanoshells and resonant Raman reporters to generate SERS tags with strong enhancements at wavelengths greater than 1000 nm [48,50,61,62]. Specifically, their SERS tags were able to achieve picomolar detection sensitivities using both 1280 nm and 1550 nm excitation wavelengths [48,61]. Recently, they were able to demonstrate designs achieving 4–5 fM detection limits

using a hand-held device operating with 1064 nm excitation at 30 mW using 0.5-s acquisition [62]. These particles are promising, as they are bright enough to be useful for in-vivo spectroscopic detection. We do believe further advancements can be made on the particle to attain detection sensitivities on par with those designed for 785 nm excitation. With nanoshells, the gold layer becomes too thin when aiming for resonances in the second NIR window, effectively turning the particle into a better absorber than a scatterer [33,63]. This limits the ability of a particle to support exceptionally strong SERS signals. Thus, anisotropic nanoparticles with larger metal volumes, supporting larger scattering contributions to the extinction, are preferable.

Most recently, Lane and Nie have experimentally compared the spectral and tissue scattering properties of SERS nanoparticles between the first and the second NIR windows (Figure 3). The results show that colloidal gold nanorods are “broad-band” plasmonic nanostructures that can be used for efficient surface Raman enhancement at both 785 nm and 1064 nm excitations. The spectral intensity patterns are considerably different, most likely because the reporter molecule (IR-1061) shows a resonance effect at 1064 nm, but not at 785 nm. When the SERS nanoparticles were buried under a 4-mm thick skin tissue (ex vivo), the SERS signal intensities were dramatically attenuated, but the ex-vivo SERS spectrum in the second NIR window still faithfully reproduced the original spectrum of the SERS particles. In contrast, the SERS spectrum in the first NIR window was hardly discernable due to strong tissue scattering and interference from the skin Raman spectrum (see Figures 3C and 3D).

5. Clinical and Preclinical Studies

Preclinical evaluation of SERS nanoparticles started with a report by Zavaleta et al. [64], who examined the dynamic biodistribution behaviors of SERS tags delivered either intravenously (IV) or intrarectally (IR). Opposed to the IV administered tags, which overwhelmingly accumulated and remained in the spleen and liver for prolonged periods (> 24 hours), IR administered SERS tags were flushed naturally from the colon, where 99% of the applied dose was eliminated by fecal excretion within a 24 h period. Though this work was expanded upon by Thakor et al. [65], who performed an extensive toxicity analysis demonstrating IV administered SERS tags elicited no significant toxicity within a 2 week period, the particles remaining in the body are still a concern as they are no longer performing a useful operation once the imaging and detection applications have been completed. Therefore, longer term studies examining the clearance and chronic toxicity of IV administered SERS tags is warranted. Topically applied SERS particles for gastrointestinal cancer detection may experience clinical translation sooner since they clear quickly and do not have systemic biodistributions. To advance SERS guided surgical applications, there is a need for Raman imaging systems that can scan wide areas in real time. Such instrumentation is just beginning to be explored [66,67], but yet to be available commercially. There are also promising studies developing endoscopic instrumentation that will aid in topically applied SERS tag cancer identification within gastrointestinal tracts (see Figure 4) [68–70].

6. Prospects and Future Directions

As there are a wide variety of anisotropic particles with strong resonances in the NIR spectral window, the push towards increased sensitivity for SERS has shifted towards Raman reporter development [6,48,62]. Though there are numerous dyes that can be used for SERS tags having high sensitivities in the first NIR window, the number of dyes optimized for the second window are far fewer. However, with increased interest in fluorescence imaging in the second window [10,11,71], several groups have been developing various dyes for this spectral region [22,72–76]. We note that the goal in fluorescence dye design is to create molecules that are efficient emitters; however, in the case of SERS, high fluorescence quantum yields are not needed. Thus, the so called “failed” designs of fluorophores with weak emission in the NIR-II region may still have great potential in the creation of bright SERS tags. Also, commercially available fluorophores that were previously developed for infrared dye lasers can be explored.

Since SERS nanoparticles have large surface areas for functionalization, researchers have also begun to incorporate other imaging modalities and therapeutic options in their nanoparticle designs. Therapeutic functions included photodynamic therapy [77,78], photothermal therapy [38,41,49,79–82], and chemotherapeutic delivery [46,83,84]. Other imaging modalities that have been incorporated include photoacoustic imaging [49,85–88], PET [64,89], CT [90], and MRI [81,85,91,92]. With so many options, SERS tags can be tailored to solve multiple biomedical imaging and therapeutic issues. However, a significant hurdle remaining within in vivo research is to move towards human studies. This will require further explorations into the long-term fate of the particles within the body [93–95].

Acknowledgments

L.A.L. acknowledges support from the 1000 National Youth Foundation of China, the Research Fellowship for International Young Scientists from the National Natural Science Foundation of China (NSFC No. 21750110440), and startup funding from Nanjing University. We also acknowledge the University of Illinois at Urbana-Champaign and the National Institutes of Health for financial support (grants R01CA163256, RC2CA148265, and HHSN268201000043C to S.N.).

References

* Special Interest

** Outstanding Interest

1*. Lane LA, Qian X, Nie S. SERS Nanoparticles in Medicine: From Label-Free Detection to Spectroscopic Tagging. Chemical Reviews. 2015; 115:10489–10529. An extensive review on the favorable optical properties of SERS and their biomedical applications. [PubMed: 26313254]

2. Cialla-May D, Zheng XS, Weber K, Popp J. Recent progress in surface-enhanced Raman spectroscopy for biological and biomedical applications: from cells to clinics. Chemical Society Reviews. 2017; 46:3945–3961. [PubMed: 28639667]

3. Doering WE, Nie S. Spectroscopic Tags Using Dye-Embedded Nanoparticles and Surface-Enhanced Raman Scattering. Analytical Chemistry. 2003; 75:6171–6176. [PubMed: 14615997]

4. Andreou C, Neuschmelting V, Tschaharganeh D-F, Huang C-H, Oseledchyk A, Iacono P, Karabeber H, Colen RR, Mannelli L, Lowe SW, et al. Imaging of Liver Tumors Using Surface-Enhanced Raman Scattering Nanoparticles. ACS Nano. 2016; 10:5015–5026. [PubMed: 27078225]

5. McCreery RL. Raman Spectroscopy for Chemical Analysis. John Wiley & Sons, Inc; 2005. Raman Microscopy and Imaging.

6**. Harmsen S, Bedics MA, Wall MA, Huang R, Detty MR, Kircher MF. Rational design of a chalcogenopyrylium-based surface-enhanced resonance Raman scattering nanoprobe with attomolar sensitivity. Nature Communications. 2015; 6:6570. Created SERS tags with attomolar sensitivity, the highest sensitivity reported to date.

7*. Harmsen S, Huang R, Wall MA, Karabeber H, Samii JM, Spaliviero M, White JR, Monette S, O'Connor R, Pitter KL, et al. Surface-enhanced resonance Raman scattering nanostars for high-precision cancer imaging. Science Translational Medicine. 2015; 7:271ra277–271ra277. The authors demonstrated that SERS tags were able to identify primary tumors and microscopic sattelite legions of a variety of cancers. Interestingly, they were also able to identify premalignant regions.

8**. Zavaleta C, Smith BR, Walton ID, Doering WE, Davis G, Shojaei B, Natan MJ, Gambhir SS. Multiplexed imaging of surface enhanced Raman scattering nanotags in living mice using noninvasive Raman spectroscopy. Proceedings of the National Academy of Sciences of the United States of America. 2009; 106:13511–13516. First demonstration of the multiplexing power of SERS in vivo, where they detected 10 different SERS signatures simultaneously. [PubMed: 19666578]

9. Dinish US, Balasundaram G, Chang Y, Olivo M. Actively Targeted In Vivo Multiplex Detection of Intrinsic Cancer Biomarkers Using Biocompatible SERS Nanotags. Scientific Reports. 2015; 4:4075–4075.

10*. Hong G, Antaris AL, Dai H. Near-infrared fluorophores for biomedical imaging. Nature Biomedical Engineering. 2017; 1:0010. An excellent review on fluorescent probes and optical properties of tissues in the first and second near infrared windows.

11*. Smith AM, Mancini MC, Nie S. Second window for in vivo imaging. Nature Nanotechnology. 2009; 4:710. An early commentary article summarizing the opportunities and challenges of in-vivo and intraoperative optical imaging in the second NIR window.

12. Pansare VJ, Hejazi S, Faenza WJ, Homme RKP. Review of Long-Wavelength Optical and NIR Imaging Materials: Contrast Agents, Fluorophores and Multifunctional Nano Carriers. Chemistry of Materials. 2012; 24:812–827. [PubMed: 22919122]

13. Steven LJ. Optical properties of biological tissues: a review. Physics in Medicine & Biology. 2013; 58:R37. [PubMed: 23666068]

14. Frangioni JV. In vivo near-infrared fluorescence imaging. Current Opinion in Chemical Biology. 2003; 7:626–634. [PubMed: 14580568]

15**. Qian X, Peng X-H, Ansari DO, Yin-Goen Q, Chen GZ, Shin DM, Yang L, Young AN, Wang MD, Nie S. In vivo tumor targeting and spectroscopic detection with surface-enhanced Raman nanoparticle tags. Nature Biotechnology. 2007; 26:83. A breakthrough paper that reported for the first time in-vivo SERS detection of solid tumors in live animal models in the first NIR window.

16. Pirollo KF, Chang EH. Does a targeting ligand influence nanoparticle tumor localization or uptake? Trends in Biotechnology. 2008; 26:552–558. [PubMed: 18722682]

17. Maeda H. Macromolecular therapeutics in cancer treatment: The EPR effect and beyond. Journal of Controlled Release. 2012; 164:138–144. [PubMed: 22595146]

18. Lane LA, Qian X, Smith AM, Nie S. Physical Chemistry of Nanomedicine: Understanding the Complex Behaviors of Nanoparticles in Vivo. Annual Review of Physical Chemistry. 2015; 66:521–547.

19. Mohs AM, Mancini MC, Singhal S, Provenzale JM, Leylandjones B, Wang MD, Nie S. Hand-held Spectroscopic Device for In Vivo and Intraoperative Tumor Detection: Contrast Enhancement, Detection Sensitivity, and Tissue Penetration. Analytical Chemistry. 2010; 82:9058–9065. [PubMed: 20925393]

20. Karabeber H, Huang R, Iacono P, Samii JM, Pitter KL, Holland EC, Kircher MF. Guiding brain tumor resection using surface-enhanced Raman scattering nanoparticles and a hand-held Raman scanner. ACS Nano. 2014; 8:9755–9766. [PubMed: 25093240]

21. Onda N, Kimura M, Yoshida T, Shibutani M. Preferential tumor cellular uptake and retention of indocyanine green for in vivo tumor imaging. International Journal of Cancer. 2016; 139:673–682. [PubMed: 27006261]
22. Antaris AL, Chen H, Cheng K, Sun Y, Hong G, Qu C, Diao S, Deng Z, Hu X, Zhang B, et al. A small-molecule dye for NIR-II imaging. Nature Materials. 2015; 15:235. [PubMed: 26595119]
23. Bashkatov AN, Genina EA, Kochubey VI, Tuchin VV. Optical properties of human skin, subcutaneous and mucous tissues in the wavelength range from 400 to 2000 nm. Journal of Physics D: Applied Physics. 2005; 38:2543.
24. Culha M, Cullum B, Lavrik N, Klutse CK. Surface-Enhanced Raman Scattering as an Emerging Characterization and Detection Technique. Journal of Nanotechnology. 2012; 2012:15.
25. Welsher K, Sherlock SP, Dai H. Deep-Tissue Anatomical Imaging of Mice Using Carbon Nanotube Fluorophores in the Second Near Infrared Window. Proceedings of the National Academy of Sciences of the United States of America. 2011; 108:8943–8948. [PubMed: 21576494]
26. Chen Y, Montana DM, Wei H, Cordero JM, Schneider M, Le Guével X, Chen O, Bruns OT, Bawendi MG. Shortwave Infrared in Vivo Imaging with Gold Nanoclusters. Nano Letters. 2017; 17:6330–6334. [PubMed: 28952734]
27. Lim YT, Kim S, Nakayama A, Stott NE, Bawendi MG, Frangioni JV. Selection of quantum dot wavelengths for biomedical assays and imaging. Molecular Imaging. 2003; 2:50–64. [PubMed: 12926237]
28. National Institute of Standards and Technology. 2007. Z136.1
29. Diao S, Hong G, Antaris AL, Blackburn JL, Cheng K, Cheng Z, Dai H. Biological Imaging without Autofluorescence in the Second Near-Infrared Region. Nano Research. 2015; 8:3027–3034.
30. Villa I, Vedda A, Cantarelli IX, Pedroni M, Piccinelli F, Bettinelli M, Speghini A, Quintanilla M, Vetrone F, Rocha U, et al. 1.3 μm emitting SrF2:Nd3+ nanoparticles for high contrast in vivo imaging in the second biological window. Nano Research. 2015; 8:649–665.
31. del Rosal B, Villa I, Jaque D, Sanz-Rodríguez F. In vivo autofluorescence in the biological windows: the role of pigmentation. Journal of Biophotonics. 2016; 9:1059–1067. [PubMed: 26576035]
32**. Nie S, Emory SR. Probing Single Molecules and Single Nanoparticles by Surface-Enhanced Raman Scattering. Science. 1997; 275:1102–1106. First report showing that SERS enhancements can reach 10^{14}, generating signals strong enough to detect a single molecule at room temperature in the condensed phase. [PubMed: 9027306]
33. Jain PK, Lee KS, Elsayed IH, Elsayed MA. Calculated Absorption and Scattering Properties of Gold Nanoparticles of Different Size, Shape, and Composition: Applications in Biological Imaging and Biomedicine. Journal of Physical Chemistry B. 2006; 110:7238–7248.
34. Li N, Zhao P, Astruc D. Anisotropic Gold Nanoparticles: Synthesis, Properties, Applications, and Toxicity. Angewandte Chemie. 2014; 53:1756–1789. [PubMed: 24421264]
35. Yang X, Yang M, Pang B, Vara M, Xia Y. Gold Nanomaterials at Work in Biomedicine. Chemical Reviews. 2015; 115:10410–10488. [PubMed: 26293344]
36. Reguera J, Langer J, Jimenez de Aberasturi D, Liz-Marzan LM. Anisotropic metal nanoparticles for surface enhanced Raman scattering. Chemical Society Reviews. 2017; 46:3866–3885. [PubMed: 28447698]
37. Park J-E, Kim M, Hwang J-H, Nam J-M. Golden Opportunities: Plasmonic Gold Nanostructures for Biomedical Applications based on the Second Near-Infrared Window. Small Methods. 2017; 1:1600032. n/a.
38. Von Maltzahn G, Centrone A, Park J, Ramanathan R, Sailor MJ, Hatton TA, Bhatia SN. SERS-Coded Gold Nanorods as a Multifunctional Platform for Densely Multiplexed Near-Infrared Imaging and Photothermal Heating. Advanced Materials. 2009; 21:3175–3180. [PubMed: 20174478]
39. Sivapalan ST, DeVetter BM, Yang TK, van Dijk T, Schulmerich MV, Carney PS, Bhargava R, Murphy CJ. Off-Resonance Surface-Enhanced Raman Spectroscopy from Gold Nanorod Suspensions as a Function of Aspect Ratio: Not What We Thought. ACS Nano. 2013; 7:2099–2105. [PubMed: 23438342]

40. Ye X, Zheng C, Chen J, Gao Y, Murray CB. Using binary surfactant mixtures to simultaneously improve the dimensional tunability and monodispersity in the seeded growth of gold nanorods. Nano Letters. 2013; 13:765–771. [PubMed: 23286198]
41. Feng J, Chen L, Xia Y, Xing J, Li Z, Qian Q, Wang Y, Wu A, Zeng L, Zhou Y. Bioconjugation of Gold Nanobipyramids for SERS Detection and Targeted Photothermal Therapy in Breast Cancer. ACS Biomaterials Science & Engineering. 2017; 3:608–618.
42. Sánchez-Iglesias A, Winckelmans N, Altantzis T, Bals S, Grzelczak M, Liz-Marzán LM. High-Yield Seeded Growth of Monodisperse Pentatwinned Gold Nanoparticles through Thermally Induced Seed Twinning. Journal of the American Chemical Society. 2017; 139:107–110. [PubMed: 28009166]
43. Li Q, Zhuo X, Li S, Ruan Q, Xu Q, Wang J. Production of Monodisperse Gold Nanobipyramids with Number Percentages Approaching 100% and Evaluation of Their Plasmonic Properties. Advanced Optical Materials. 2015; 3:801–812.
44. Rycenga M, Wang Z, Gordon E, Cobley CM, Schwartz AG, Lo CS, Xia Y. Probing the Photothermal Effect of Gold-Based Nanocages with Surface-Enhanced Raman Scattering (SERS). Angewandte Chemie International Edition. 2009; 48:9924–9927. [PubMed: 20014343]
45. Hu F, Zhang Y, Chen G, Li C, Wang Q. Double-Walled Au Nanocage/SiO2 Nanorattles: Integrating SERS Imaging, Drug Delivery and Photothermal Therapy. Small. 2015; 11:985–993. [PubMed: 25348096]
46. Tian L, Gandra N, Singamaneni S. Monitoring Controlled Release of Payload from Gold Nanocages Using Surface Enhanced Raman Scattering. ACS Nano. 2013; 7:4252–4260. [PubMed: 23577650]
47. Moreton S, Faulds K, Shand NC, Bedics MA, Detty MR, Graham D. Functionalisation of hollow gold nanospheres for use as stable, red-shifted SERS nanotags. Nanoscale. 2015; 7:6075–6082. [PubMed: 25766131]
48. Bedics MA, Kearns H, Cox JM, Mabbott S, Ali F, Shand NC, Faulds K, Benedict JB, Graham D, Detty MR. Extreme red shifted SERS nanotags. Chemical Science. 2015; 6:2302–2306. [PubMed: 29308144]
49. Song J, Yang X, Yang Z, Lin L, Liu Y, Zhou Z, Shen Z, Yu G, Dai Y, Jacobson O, et al. Rational Design of Branched Nanoporous Gold Nanoshells with Enhanced Physico-Optical Properties for Optical Imaging and Cancer Therapy. ACS Nano. 2017; 11:6102–6113. [PubMed: 28605594]
50*. Kearns H, Shand NC, Smith WE, Faulds K, Graham D. 1064 nm SERS of NIR active hollow gold nanotags. Physical Chemistry Chemical Physics. 2015; 17:1980–1986. Here the authors developed SERS tags having femtomolar senitivity within the second near infrared window. [PubMed: 25475892]
51. Scarabelli L, Coronado-Puchau M, Giner-Casares JJ, Langer J, Liz-Marzán LM. Monodisperse Gold Nanotriangles: Size Control, Large-Scale Self-Assembly, and Performance in Surface-Enhanced Raman Scattering. ACS Nano. 2014; 8:5833–5842. [PubMed: 24848669]
52. Qin F, Zhao T, Jiang R, Jiang N, Ruan Q, Wang J, Sun L-D, Yan C-H, Lin H-Q. Thickness Control Produces Gold Nanoplates with Their Plasmon in the Visible and Near-Infrared Regions. Advanced Optical Materials. 2016; 4:76–85.
53. Millstone JE, Hurst SJ, Metraux GS, Cutler JI, Mirkin CA. Colloidal Gold and Silver Triangular Nanoprisms. Small. 2009; 5:646–664. [PubMed: 19306458]
54. Indrasekara ASDS, Meyers S, Shubeita S, Feldman LC, Gustafsson T, Fabris L. Gold nanostar substrates for SERS-based chemical sensing in the femtomolar regime. Nanoscale. 2014; 6:8891–8899. [PubMed: 24961293]
55. Register JK, Fales AM, Wang H, Norton SJ, Cho EH, Boico A, Pradhan S, Kim JS, Schroeder T, Wisniewski NA. In vivo detection of SERS-encoded plasmonic nanostars in human skin grafts and live animal models. Analytical and Bioanalytical Chemistry. 2015; 407:8215–8224. [PubMed: 26337748]
56. Huang R, Harmsen S, Samii JM, Karabeber H, Pitter KL, Holland EC, Kircher MF. High Precision Imaging of Microscopic Spread of Glioblastoma with a Targeted Ultrasensitive SERRS Molecular Imaging Probe. Theranostics. 2016; 6:1075–1084. [PubMed: 27279902]

57. Nayak TR, Andreou C, Oseledchyk A, Marcus WD, Wong HC, Massague J, Kircher MF. Tissue factor-specific ultra-bright SERRS nanostars for Raman detection of pulmonary micrometastases. Nanoscale. 2017; 9:1110–1119. [PubMed: 27991632]

58. Harmsen S, Huang R, Wall MA, Karabeber H, Samii JM, Spaliviero M, White Monette S, Oconnor R, Pitter KL. Surface-Enhanced Resonance Raman Scattering Nanostars for High Precision Cancer Imaging. Science Translational Medicine. 2015:7.

59. Gandra N, Hendargo HC, Norton SJ, Fales AM, Palmer GM, Vodinh T. Tunable and amplified Raman gold nanoprobes for effective tracking (TARGET): in vivo sensing and imaging. Nanoscale. 2016; 8:8486–8494. [PubMed: 27064259]

60. Shen W, Lin X, Jiang C, Li C, Lin H, Huang J, Wang S, Liu G, Yan X, Zhong Q. Reliable Quantitative SERS Analysis Facilitated by Core–Shell Nanoparticles with Embedded Internal Standards. Angewandte Chemie. 2015; 54:7308–7312. [PubMed: 25939998]

61. Kearns H, Bedics MA, Shand NC, Faulds K, Detty MR, Graham D. Sensitive SERS nanotags for use with 1550 nm (retina-safe) laser excitation. Analyst. 2016; 141:5062–5065. [PubMed: 26788554]

62. Kearns H, Ali F, Bedics MA, Shand NC, Faulds K, Detty MR, Graham D. Sensitive SERS nanotags for use with a hand-held 1064 nm Raman spectrometer. Royal Society Open Science. 2017:4.

63. Oldenburg SJ, Jackson JB, Westcott SL, Halas NJ. INFRARED EXTINCTION PROPERTIES OF GOLD NANOSHELLS. Applied Physics Letters. 1999; 75:2897–2899.

64**. Zavaleta C, Hartman KB, Miao Z, James ML, Kempen P, Thakor AS, Nielsen CH, Sinclair R, Cheng Z, Gambhir SS. Preclinical Evaluation of Raman Nanoparticle Biodistribution for their Potential Use in Clinical Endoscopy Imaging. Small. 2011; 7:2232–2240. First report showing topically applied SERS nanoparticles within the gastrointestinal tracts may have sooner clinical approval than intravenously administered particles. The topically applied particles quickly exited the colon and were not able to enter the blood stream. [PubMed: 21608124]

65*. Thakor AS, Luong R, Paulmurugan R, Lin FI, Kempen P, Zavaleta C, Chu P, Massoud TF, Sinclair R, Gambhir SS. The Fate and Toxicity of Raman-Active Silica-Gold Nanoparticles in Mice. Science Translational Medicine. 2011; 3:79ra33–79ra33. As extensive study on the fate and toxicity of topically and intravenously administered SERS nanoparticles.

66*. Bohndiek SE, Wagadarikar A, Zavaleta CL, Van de Sompel D, Garai E, Jokerst JV, Yazdanfar S, Gambhir SS. A small animal Raman instrument for rapid, wide-area, spectroscopic imaging. Proceedings of the National Academy of Sciences. 2013; 110:12408–12413. A promising direction for the development of wide-field Raman imaging devices to detect SERS particles rapidly over wider regions of tissues.

67. Papour A, Kwak JH, Taylor Z, Wu B, Stafsudd O, Grundfest W. Wide-field Raman imaging for bone detection in tissue. Biomedical Optics Express. 2015; 6:3892–3897. [PubMed: 26504639]

68*. Garai E, Sensarn S, Zavaleta C, Loewke NO, Rogalla S, Mandella MJ, Felt SA, Friedland S, Liu JTC, Gambhir SS. A Real-Time Clinical Endoscopic System for Intraluminal, Multiplexed Imaging of Surface-Enhanced Raman Scattering Nanoparticles. PLOS ONE. 2015:10. A promising endoscopic device for the rapid and sensitive detection of topicaly applied SERS tags within gastrointestinal tracts.

69. Wang YW, Kang S, Khan A, Bao PQ, Liu JTC. In vivo multiplexed molecular imaging of esophageal cancer via spectral endoscopy of topically applied SERS nanoparticles. Biomedical Optics Express. 2015; 6:3714–3723. [PubMed: 26504623]

70. Wang YW, Khan A, Leigh SY, Wang D, Chen Y, Meza D, Liu JTC. Comprehensive spectral endoscopy of topically applied SERS nanoparticles in the rat esophagus. Biomedical Optics Express. 2014; 5:2883–2895. [PubMed: 25401005]

71. Zhao J, Zhong D, Zhou S. NIR-I-to-NIR-II fluorescent nanomaterials for biomedical imaging and cancer therapy. Journal of Materials Chemistry B. 2018

72. Cosco ED, Caram JR, Bruns OT, Franke D, Day RA, Farr EP, Bawendi MG, Sletten EM. Flavylium Polymethine Fluorophores for Near- and Shortwave Infrared Imaging. Angewandte Chemie International Edition. 2017; 56:13126–13129. [PubMed: 28806473]

73. Sun Y, Ding M, Zeng X, Xiao Y, Wu H, Zhou H, Ding B, Qu C, Hou W, Er-bu AGA, et al. Novel bright-emission small-molecule NIR-II fluorophores for in vivo tumor imaging and image-guided surgery. Chemical Science. 2017; 8:3489–3493. [PubMed: 28507722]
74. Sun Y, Qu C, Chen H, He M, Tang C, Shou K, Hong S, Yang M, Jiang Y, Ding B, et al. Novel benzo-bis(1,2,5-thiadiazole) fluorophores for in vivo NIR-II imaging of cancer. Chemical Science. 2016; 7:6203–6207. [PubMed: 30034761]
75. Zhang X, Wang H, Antaris AL, Li L, Diao S, Ma R, Nguyen A, Hong G, Ma Z, Wang J. Traumatic Brain Injury Imaging in the Second Near-Infrared Window with a Molecular Fluorophore. Advanced Materials. 2016; 28:6872–6879. [PubMed: 27253071]
76. Yang Q, Hu Z, Zhu S, Ma R, Ma H, Ma Z, Wan H, Zhu T, Jiang Z, Liu W, et al. Donor Engineering for NIR-II Molecular Fluorophores with Enhanced Fluorescent Performance. Journal of the American Chemical Society. 2018
77. Zhang Y, Qian J, Wang D, Wang Y, He S. Multifunctional Gold Nanorods with Ultrahigh Stability and Tunability for In Vivo Fluorescence Imaging, SERS Detection, and Photodynamic Therapy. Angewandte Chemie International Edition. 2013; 52:1148–1151. [PubMed: 23233455]
78. Fales AM, Crawford BM, Vo-Dinh T. Folate Receptor-Targeted Theranostic Nanoconstruct for Surface-Enhanced Raman Scattering Imaging and Photodynamic Therapy. ACS Omega. 2016; 1:730–735. [PubMed: 30023488]
79. Lu W, Singh AK, Khan SA, Senapati D, Yu H, Ray PC. Gold Nano-Popcorn-Based Targeted Diagnosis, Nanotherapy Treatment, and In Situ Monitoring of Photothermal Therapy Response of Prostate Cancer Cells Using Surface-Enhanced Raman Spectroscopy. Journal of the American Chemical Society. 2010; 132:18103–18114. [PubMed: 21128627]
80. Seo S, Kim B, Joe A, Han H, Chen X, Cheng Z, Jang E. NIR-light-induced surface-enhanced Raman scattering for detection and photothermal/photodynamic therapy of cancer cells using methylene blue-embedded gold nanorod@SiO2 nanocomposites. Biomaterials. 2014; 35:3309–3318. [PubMed: 24424205]
81. Gao Y, Li Y, Chen J, Zhu S, Liu X, Zhou L, Shi P, Niu D, Gu J, Shi J. Multifunctional gold nanostar-based nanocomposite: Synthesis and application for noninvasive MR-SERS imaging-guided photothermal ablation. Biomaterials. 2015; 60:31–41. [PubMed: 25982551]
82. Liu Y, Ashton JR, Moding EJ, Yuan H, Register JK, Fales AM, Choi J, Whitley MJ, Zhao X, Qi Y. A Plasmonic Gold Nanostar Theranostic Probe for In Vivo Tumor Imaging and Photothermal Therapy. Theranostics. 2015; 5:946–960. [PubMed: 26155311]
83. Hu F, Zhang Y, Chen G, Li C, Wang Q. Double-Walled Au Nanocage/SiO2 Nanorattles: Integrating SERS Imaging, Drug Delivery and Photothermal Therapy. Small. 2015; 11:985–993. [PubMed: 25348096]
84. Tian F, Conde J, Bao C, Chen Y, Curtin J, Cui D. Gold nanostars for efficient in vitro and in vivo real-time SERS detection and drug delivery via plasmonic-tunable Raman/FTIR imaging. Biomaterials. 2016; 106:87–97. [PubMed: 27552319]
85*. Kircher MF, La Zerda AD, Jokerst JV, Zavaleta C, Kempen P, Mittra E, Pitter KL, Huang R, Campos C, Habte F. A brain tumor molecular imaging strategy using a new triple-modality MRI-photoacoustic-Raman nanoparticle. Nature Medicine. 2012; 18:829–834. A prime example of integrating multiple imaging functionalities into a single SERS probe for in vivo cancer imaging and detection.
86. Cha MG, Lee S, Park S, Kang H, Lee SG, Jeong C, Lee Y-S, Kim C, Jeong DH. A dual modal silver bumpy nanoprobe for photoacoustic imaging and SERS multiplexed identification of in vivo lymph nodes. Nanoscale. 2017; 9:12556–12564. [PubMed: 28820223]
87. Jokerst JV, Cole AJ, De Sompel DV, Gambhir SS. Gold nanorods for ovarian cancer detection with photoacoustic imaging and resection guidance via Raman imaging in living mice. ACS Nano. 2012; 6:10366–10377. [PubMed: 23101432]
88. Dinish US, Song Z, Ho CJH, Balasundaram G, Attia ABE, Lu X, Tang BZ, Liu B, Olivo M. Single Molecule with Dual Function on Nanogold: Biofunctionalized Construct for In Vivo Photoacoustic Imaging and SERS Biosensing. Advanced Functional Materials. 2015; 25:2316–2325.

89. Wall AM, Shaffer MT, Harmsen S, Tschaharganeh D-F, Huang C-H, Lowe WS, Drain CF, Kircher M. Chelator-Free Radiolabeling of SERRS Nanoparticles for Whole-Body PET and Intraoperative Raman Imaging. 2017; 7

90. Xiao M, Nyagilo JO, Arora V, Kulkarni PV, Xu D, Sun X, Dave DP. Gold nanotags for combined multi-colored Raman spectroscopy and x-ray computed tomography. Nanotechnology. 2010; 21:035101. [PubMed: 19966403]

91. Yigit MV, Zhu L, Ifediba MA, Zhang Y, Carr K, Moore A, Medarova Z. Noninvasive MRI-SERS imaging in living mice using an innately bimodal nanomaterial. ACS Nano. 2011; 5:1056–1066. [PubMed: 21194236]

92. Gao X, Yue Q, Liu Z, Ke M, Zhou X, Li S, Zhang J, Zhang R, Chen L, Mao Y, et al. Guiding Brain-Tumor Surgery via Blood–Brain-Barrier-Permeable Gold Nanoprobes with Acid-Triggered MRI/SERRS Signals. Advanced Materials. 2017; 29:1603917. n/a.

93. Yu M, Zheng J. Clearance Pathways and Tumor Targeting of Imaging Nanoparticles. ACS Nano. 2015; 9:6655–6674. [PubMed: 26149184]

94. Zhang Y, Poon W, Tavares AJ, Mcgilvray ID, Chan WCW. Nanoparticle–liver interactions: Cellular uptake and hepatobiliary elimination. Journal of Controlled Release. 2016; 240:332–348. [PubMed: 26774224]

95. Feliu N, Docter D, Heine M, Pino PD, Ashraf S, Kolosnjajtabi J, Macchiarini P, Nielsen P, Alloyeau D, Gazeau F. In vivo degeneration and the fate of inorganic nanoparticles. Chemical Society Reviews. 2016; 45:2440–2457. [PubMed: 26862602]

Highlights

- The first clear window, defined as light wavelengths between 650 nm and 950 nm, is far superior for in-vivo and intraoperative optical imaging than visible light.
- The second clear window, operating in the wavelength range of 1000 nm to 1700 nm, can further improve detection sensitivity, spatial resolution, and tissue penetration due to reduced light scattering and background interference.
- Surface-enhanced Raman scattering (SERS), based on biocompatible plasmonic nanoparticles, allows in-vivo and intraoperative spectroscopy both in the first and second NIR windows.
- The major advantages of SERS nanoparticle tags include improved photostability, detection sensitivity, and spectral multiplexing capability.
- New reporter dyes and advanced instrumentation have started to emerge for SERS studies in the second NIR window.
- Further studies are needed to understand the in-vivo fate and long-term safety/toxicity of encoded SERS nanoparticles.

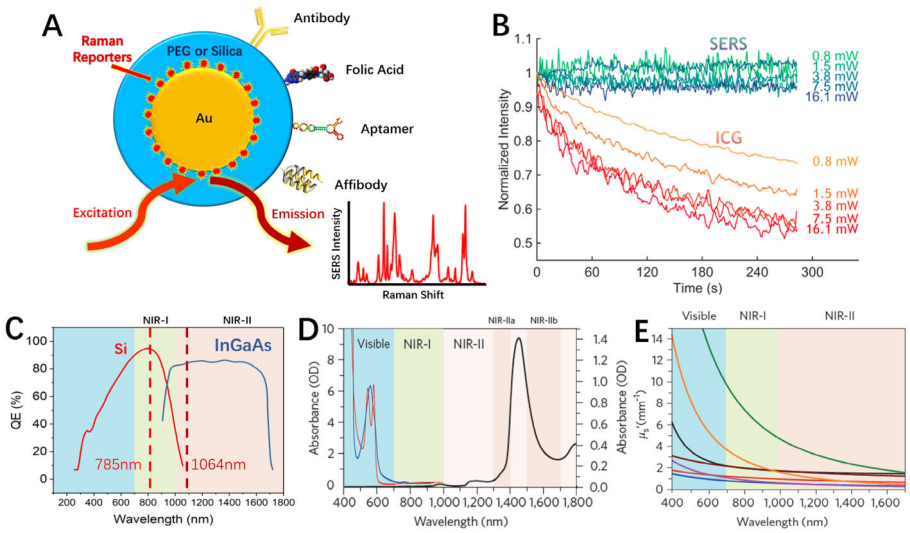

Figure 1.

(A) Schematic diagram of biocompatible surface-enhanced Raman scattering (SERS) nanoparticles that are encoded with Raman reporter molecules and conjugated with targeting ligands for in-vivo and intraoperative cancer detection. (B) Graphs comparing the photostability between SERS tags and indocyanine green (ICG) at various laser excitation powers. ICG is a common organic fluorophore used in fluorescence image-guided surgery. (C–E) Emergence of two windows in the near infrared (NIR) for in-vivo imaging and spectroscopic detection. (C) Sensitivity curves for typical cameras based on silicon (Si) or indium gallium arsenide (InGaAs), which are sensitive in the first and second near-infrared windows, respectively. The excitation wavelengths at 785 nm and 1064 nm are indicated by vertical dotted lines. (D) Absorbance of oxygenated (red curve) and deoxygenated (blue curve) hemoglobin in the visible and NIR spectrum, together with water absorbance (black curve) at 1400–1500 nm. (E) Plots of the scattering attenuation coefficient as a function of wavelength for various ex-vivo tissues (from top to bottom: green curve = brain tissue, yellow curve = intralipid tissue phantom, black curve = skin, brown curve = cranial bone, purple curve =mucous tissue, red curve =subcutaneous tissue, blue curve = muscle tissue). (B) and (D & E) were adapted with permission from references [4] and [10], respectively.

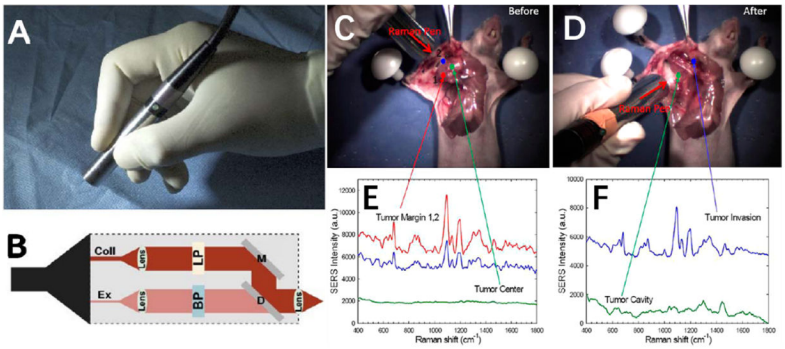

Figure 2.

(A) Photograph of a handheld spectroscopic device called the “Raman Pen” for high-sensitivity detection of tumor margins, metastatic lymph nodes, and micro-metastases during surgery. (B) Optical layout of the pen device: Ex = excitation fiber, Coll = collection fiber, BP = bandpass filter, LP = long-pass filter, D= dichroic mirror, M = total reflection mirror. (C–F) Demonstration of spectroscopic guided surgical resection of a tumor using SERS nanoparticle tags and a hand-held spectroscopic device. (C) Photograph of the anatomical locations where SERS spectra were obtained, shown in (E), across a xenograft tumor prior to resection. (D) Photograph of the anatomical locations where the SERS spectra were obtained, shown in (F), across the tumor cavity and surrounding areas after tumor resection. Note that scanning areas outside of the primary tumor location lead to a surprise finding of a satellite micrometastatic legion that would have otherwise gone unnoticed by the surgeon. (A&B) and (C–F) were adapted with permission from references [19] and [1], respectively.

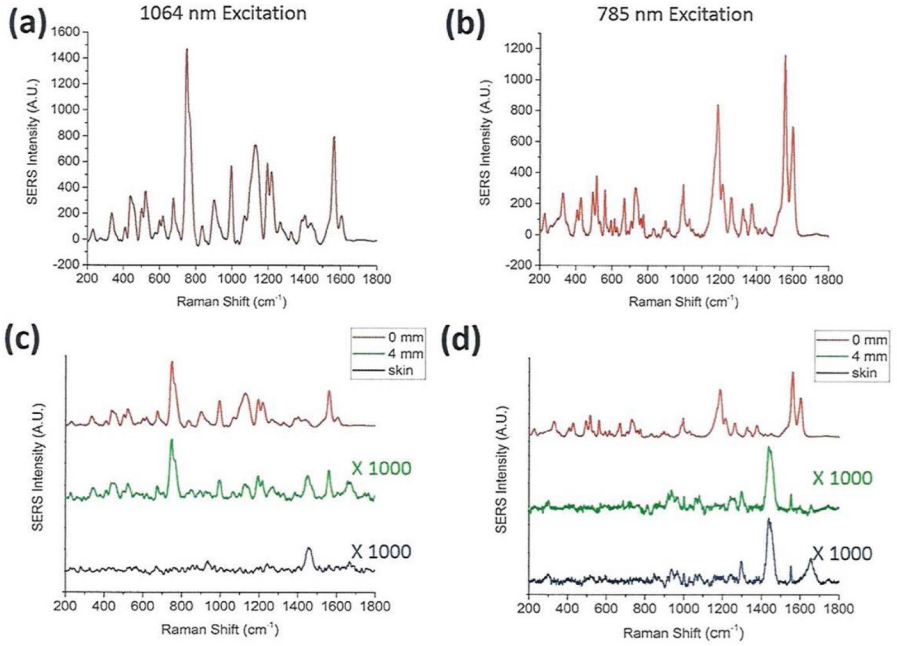

Figure 3.

Direct comparison of SERS signals and tissue penetration properties for broad-band plasmonic nanoparticles between the first and the second NIR windows. (A) and (B): SERS spectra of colloidal gold nanoparticles encoded with an IR dye at 1064 nm and 785 nm laser excitations, respectively. (C) and (D): Raman spectra of SERS nanoparticles without tissue attenuation (0 mm tissue thickness, red curves), covered with a 4-mm thick skin tissue ex vivo (green curves), together with the normal Raman scattering spectra of fresh ex-vivo pig skin (black curves). Laser wavelength: 1064 nm in (C) and 785 nm in (D). The label x1000 in (C) and (D) indicates that the intensity scale (Y-axis) is expanded by 1000-fold, which is needed to reveal detailed spectral features under tissue scattering/signal attenuation conditions. Figure Credits: Lucas A. Lane and Shuming Nie.

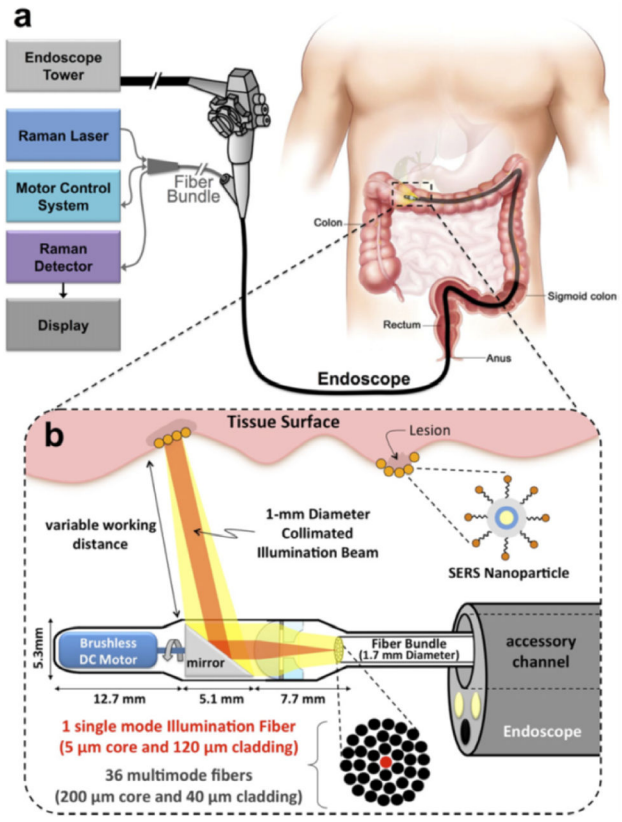

Figure 4.

Design of an endoscopic system for Intraluminal, multiplexed detection of SERS nanoparticles in the GI tract. Adapted with permission from reference [68].